

Learning and Discovering Quantum Properties with Multi-Task Neural Networks

Ya-Dong Wu,¹ Yan Zhu,^{1,*} Yuexuan Wang,^{2,3} and Giulio Chiribella^{1,4,5,†}

¹*QICI Quantum Information and Computation Initiative, Department of Computer Science,
The University of Hong Kong, Pokfulam Road, Hong Kong*

²*AI Technology Lab, Department of Computer Science,
The University of Hong Kong, Pokfulam Road, Hong Kong*

³*College of Computer Science and Technology, Zhejiang University, Zhejiang Province, China*

⁴*Department of Computer Science, Parks Road, Oxford, OX1 3QD, United Kingdom*

⁵*Perimeter Institute for Theoretical Physics, Waterloo, Ontario N2L 2Y5, Canada*

Deep neural networks are a powerful tool for predicting properties of quantum states from limited measurement data. Here we develop a network model that can simultaneously predict multiple quantum properties, including not only expectation values of quantum observables, but also general nonlinear functions of the quantum state, like entanglement entropies and many-body topological invariants. Remarkably, we find that a model trained on a given set of properties can also discover new properties outside that set. Multi-purpose training also enables the model to infer global properties of many-body quantum systems from local measurements, to classify symmetry protected topological phases of matter, and to discover unknown boundaries between different phases.

I. INTRODUCTION

Characterizing unknown quantum states from experimental data is an essential task for quantum information and quantum computation. Neural networks provide a powerful approach to quantum state characterization [1–4], enabling a compact representation of sufficiently structured quantum states [5]. In recent years, different types of neural networks have been successfully utilized to predict properties of quantum systems, including quantum fidelity [6], quantum similarity [7], quantum entanglement [8–10], entanglement entropy [1, 11, 12], two-point correlations [1, 2, 11, 13] and Pauli expectation values [4, 14], as well as to identify phases of matter [15–18].

A limitation of the existing models, however, is that they train neural networks specifically for one type of property, but cannot generalize to other types of properties directly once the training is concluded. For example, a network trained to predict the statistics of a given set of quantum observables cannot be directly used to estimate the entanglement entropy or other non-linear properties of the quantum state. Rather than re-training the model for different properties, it would be desirable to have a unified model that learns multiple properties simultaneously. Moreover, the opportunity to combine clues from different properties could potentially yield a more efficient characterization of quantum states from limited measurement data.

In this paper, we present the first neural network model for simultaneously predicting multiple properties of quantum systems. Our model employs multi-task learning [19], a technique in classical machine learning that has been successfully applied to natural language

processing tasks such as semantics analysis, translation, text prediction, and chatbots. In the quantum domain, multi-task learning endows our model with an ability to generate state representations that integrate different types of information and enable precise predictions even with data from restricted sets of measurements. For example, we find that our model can effectively learn global features of many-body quantum states, such string order parameters and many-body topological invariants [20], from the outcomes of local measurements on a few neighboring spins.

Remarkably, a model trained on a given set of properties can also discover new properties outside that set. For example, the data-driven state representations produced by our network can also be used for unsupervised classification of distinct symmetry protected topological (SPT) phases [21, 22] without the need of providing any label of the phase of matter during training. To highlight this point, we develop the first classical algorithm for classifying SPT phases directly from measurement data, instead of reconstructing reduced density matrices on local subsystems [23–25]. Finally, we show that the state representations produced by our network can also be used to discover the boundaries between different quantum phases.

II. RESULTS

Framework. Consider the scenario where an experimenter has access to multiple copies of an unknown quantum state ρ_θ , characterized by some physical parameters θ . For example, ρ_θ could be a ground state of many-body Hamiltonian with unknown parameters θ . The experimenter’s goal is to predict a set of properties of the quantum state, such as the expectation values of some observables, or some nonlinear functions, such as the von Neumann entropy. The experimenter is able to perform a restricted set of quantum measurements, denoted by \mathcal{M} .

* yzhu2@cs.hku.hk; Ya-Dong Wu and Yan Zhu contribute equally

† giulio@cs.hku.hk

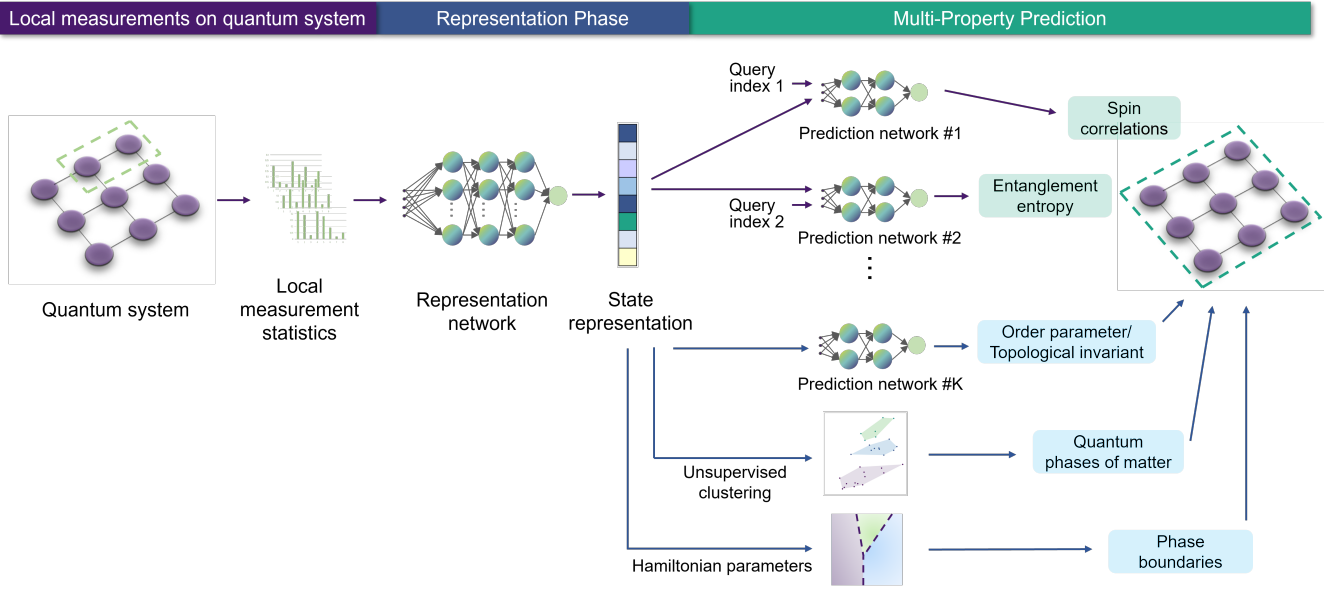


Figure 1. Flowchart of our neural network model for predicting multiple properties of a quantum system. In the data acquisition phase, the experimenter performs quantum measurements on local subsystems and collects the outcome data. In the state representation phase, a representation network produces a concise data-driven representation of the quantum state. Finally, in the multi-property prediction phase each prediction network produces predictions of a quantum property, such as a spin correlations, and entanglement entropy, or and order parameter. The state representations can also be used for unsupervised classification of quantum phases of matter and for discovering unknown phase boundaries.

Each measurement $\mathbf{M} \in \mathcal{M}$ is described by a positive operator-valued measure (POVM) $\mathbf{M} = (M_j)$, where the index j labels the measurement outcome, each M_j is a positive operator acting on the system's Hilbert space, and the normalization condition $\sum_j M_j = I$ is satisfied. In general, the measurement set \mathcal{M} may not be informationally complete. For multipartite systems, it will typically consist of local measurements, which are easier to perform in the laboratory.

To collect data, the experimenter randomly picks a subset of measurements $\mathcal{S} \subset \mathcal{M}$, and performs them on different copies of the state ρ_θ . We will denote by s the number of measurements in \mathcal{S} , and by $\mathbf{M}_i := (M_{ij})$ the i -th POVM in \mathcal{S} . For simplicity, we assume that each measurement in \mathcal{S} is repeated sufficiently many times, so that the experimenter can reliably estimate the outcome distribution $\mathbf{d}_i := (d_{ij})$, where $d_{ij} := \text{tr}(\rho M_{ij})$.

The experimenter will then try to predict multiple quantum properties of ρ_θ using the outcome distributions $(\mathbf{d}_i)_{i=1}^s$. This task is achieved by a neural network that consists of an encoder and multiple decoders, where the encoder \mathcal{E} produces a representation of quantum states and the k -th decoder \mathcal{D}_k produces a prediction of the k -th property of interest. Due to their roles, the encoder and decoders are also known as representation and prediction networks, respectively. The input of the representation network \mathcal{E} is the outcome distribution \mathbf{d}_i , together with a parametrization of the corresponding measurement \mathbf{M}_i , hereafter denoted by \mathbf{m}_i . From the pair of data $(\mathbf{d}_i, \mathbf{m}_i)$, the network produces a state representation

$\mathbf{r}_i := \mathcal{E}(\mathbf{d}_i, \mathbf{m}_i)$. To combine the state representations arising from different measurements in \mathcal{S} , the network computes the average $\mathbf{r} := \frac{1}{s} \sum_{i=1}^s \mathbf{r}_i$. At this point, the vector \mathbf{r} can be viewed as a representation of the unknown quantum state ρ .

Each prediction network \mathcal{D}_k is dedicated to a different property of the quantum state. In the case of multipartite quantum systems, we include the option of evaluating the property on a subsystem, specified by a parameter q . We denote by $f_{k,q}(\rho_\theta)$ the correct value of the k -th property of subsystem q when the total system is in the state ρ_θ . Upon receiving the state representation \mathbf{r} and the subsystem specification q , the prediction network produces an estimate $\mathcal{D}_k(\mathbf{r}, q)$ of the value $f_{k,q}(\rho)$.

The representation network and all the prediction networks are trained jointly, with the goal of minimizing the prediction error on a set of fiducial states. The fiducial states are chosen by randomly sampling a set of physical parameters $(\theta_l)_{l=1}^L$. For each fiducial state ρ_{θ_l} , we independently sample a set of measurements \mathcal{S}_l and calculate the outcome distributions for each measurement in the set \mathcal{S}_l . We randomly choose a subset of properties \mathcal{K}_l for each ρ_{θ_l} , where each property $k \in \mathcal{K}_l$ corresponds to a set of subsystems \mathcal{Q}_k , and then calculate the correct values of the quantum properties $\{f_{k,q}(\rho_{\theta_l})\}$ for all properties $k \in \mathcal{K}_l$ associated with subsystems $q \in \mathcal{Q}_k$. The training data may be either classically simulated or gathered by actual measurements on the set of fiducial states, or it could also be obtained by any combination of these two approaches.

During the training, we do not provide the model with any information about the physical parameters θ_l or about the functions $f_{k,q}$. Instead, the internal parameters of the neural networks are jointly optimized in order to minimize the estimation errors $|\mathcal{D}_k(1/s \sum_{i=1}^s \mathcal{E}(\{\mathbf{d}_i, \mathbf{m}_i\}), q) - f_{k,q}(\rho_\theta)|$ summed over all the fiducial states, all chosen properties, and all chosen subsystems.

After the training is concluded, our model can be used for predicting the properties of a new, unknown state ρ_θ . Summarizing, the procedure for generating the predictions consists of three steps, namely the data acquisition phase, the state representation phase, and the multi-property prediction phase. These three steps are summarized by the flow chart in Fig. 1.

One-dimensional cluster-Ising model. We first test the performance of our model on a relatively small system of $N = 9$ qubits whose states and their properties can be explicitly calculated. For the state family, we take the ground states of one-dimensional cluster-Ising model [26]

$$H = - \sum_{i=1}^{N-2} \sigma_i^z \sigma_{i+1}^x \sigma_{i+2}^z - h_1 \sum_{i=1}^N \sigma_i^x - h_2 \sum_{i=1}^{N-1} \sigma_i^x \sigma_{i+1}^x. \quad (1)$$

When $h_1 = h_2 = 0$, the ground state of this Hamiltonian becomes an ideal one-dimensional cluster state [27]

$$|\Psi\rangle := \Pi_{i=1}^{N-1} \mathbf{CZ}_{i,i+1} |+\rangle^{\otimes N}, \quad (2)$$

where $\mathbf{CZ}_{i,i+1}$ denotes controlled-Z gate acting on qubits i and $i+1$. In general, the corresponding ground state falls in one of three phases, depending on the values of the parameters (h_1, h_2) . The three phases are: the SPT phase, the paramagnetic phase, and the antiferromagnetic phase. SPT phase can be distinguished from symmetry broken phases by measuring the string order parameter [28, 29] $\langle \hat{S} \rangle := \langle \sigma_1^z \sigma_2^x \sigma_4^x \dots \sigma_{N-3}^x \sigma_{N-1}^x \sigma_N^z \rangle$, which is a global property involving all the N qubits.

We test our network model on the ground states corresponding to a 64×64 square grid in the parameter region $(h_1, h_2) \in [0, 1.6] \times [-1.6, 1.6]$. For the set of accessible measurements \mathcal{M} , we take all possible three-nearest-neighbour Pauli measurements, corresponding to the observables $\sigma_i^\alpha \otimes \sigma_{i+1}^\beta \otimes \sigma_{i+2}^\gamma$, where $i \in \{1, 2, \dots, N-2\}$ and $\alpha, \beta, \gamma \in \{x, y, z\}$.

For the prediction tasks, we consider a set of properties that includes both linear and nonlinear functions, as well as both local and nonlocal properties. Specifically, we consider: (A1) the fidelity with the cluster state (2), corresponding to the function $F(\rho, |\Psi\rangle\langle\Psi|) := \langle\Psi|\rho|\Psi\rangle$, and the overlap between the local states of a subsystem A , corresponding to the function $F_{\max}(\rho_A, \rho_A^\Psi) := \text{tr}(\rho_A \rho_A^\Psi) / \max\{\text{tr}(\rho_A^2), \text{tr}[(\rho_A^\Psi)^2]\}$, where ρ_A and ρ_A^Ψ are the reduced density matrices of ρ and ρ^Ψ , respectively; (A2) the entanglement indicator $\xi_{AB} := \text{tr}(\rho_{AB}^2) / \text{tr}\left[\left(\rho_{AB}^\top\right)^3\right]$, where A and B are nonoverlapping subsystems, and \top_A denotes the partial transpose on A (this quantity is known to be larger than

one only if the subsystems at A and B are entangled [30]); (A3) the Rényi entanglement entropy of order two $S_A := -\log_2(\text{tr} \rho_A^2)$ for subsystem $A = [1, 2, \dots, i]$, where $1 \leq i < N$, and the Rényi mutual information $I_{A:B} := S_A + S_B - S_{AB}$ for nonoverlapping subsystems A and B ; (A4) the two-point correlation function $C_{1j}^\alpha := \langle \sigma_1^\alpha \sigma_j^\alpha \rangle_\rho - \langle \sigma_1^\alpha \rangle_\rho \langle \sigma_j^\alpha \rangle_\rho$, where $1 < j \leq N$ and $\alpha = x, z$; (A5) local Pauli expectation values, i.e. magnetization $\langle \sigma_i^x \rangle_\rho$ for each $1 \leq i \leq N$ and expectation values of cluster state stabilizers $\langle \sigma_{i-1}^z \sigma_i^x \sigma_{i+1}^z \rangle_\rho$ for all $2 \leq i \leq N-1$. Properties (A1)-(A5) can all be either classically calculated or experimentally estimated by preparing the appropriate quantum state and performing randomized measurements [31].

We train our neural network with respect to the fiducial ground states corresponding to 300 randomly chosen points from our 4096-element grid. For each fiducial state, we provide the neural network with the outcome distributions of $s = 50$ measurements, randomly chosen from the 243 measurements in \mathcal{M} , and the values of at most two types of quantum properties, randomly chosen from (A1)-(A5). After training is concluded, we apply our trained model for predicting all the properties (A1)-(A5) for all remaining ground states corresponding to points on the grid. For each test state, we provide the representation network with the outcome distributions on $s = 50$ measurement settings randomly chosen from \mathcal{M} . Interestingly, our network makes accurate predictions even near to the boundary between the SPT phase and antiferromagnetic phase, in spite to the fact phase transitions typically make it more difficult to capture the ground state properties from limited measurement data. For a ground state close to the boundary, marked by a star in the phase diagram (Fig. 3b), the predictions of the entanglement entropy \mathcal{S}_A , spin correlation C_{1j}^z , quantum fidelity $F(\rho_A, \rho_A^\Psi)$ and entanglement indicator ξ_{AB} are close to the corresponding ground truths, as shown in Fig. 2b, c, d, and e respectively.

Remarkably, the state representation produced by the encoder can also be used for performing tasks that were not encountered during training. For example, we find that the state representation can be used to distinguish between the phases of matter associated to different values of the Hamiltonian parameters. To see this, we project the representations of all the test states onto a two-dimensional plane using the t-distributed stochastic neighbour embedding (t-SNE) algorithm. The results are shown in Fig. (3)a. At every data point of this 2D projection, we show the exact value of the string order parameter, which distinguishes between the SPT phase and the symmetry broken phases. Quite strikingly, the pattern of the points in the 2D representation matches the values of the string order parameter, even though no information about the string order parameters was provided during the training, and even though the string order is a global property, while all the measurements used by the network are local.

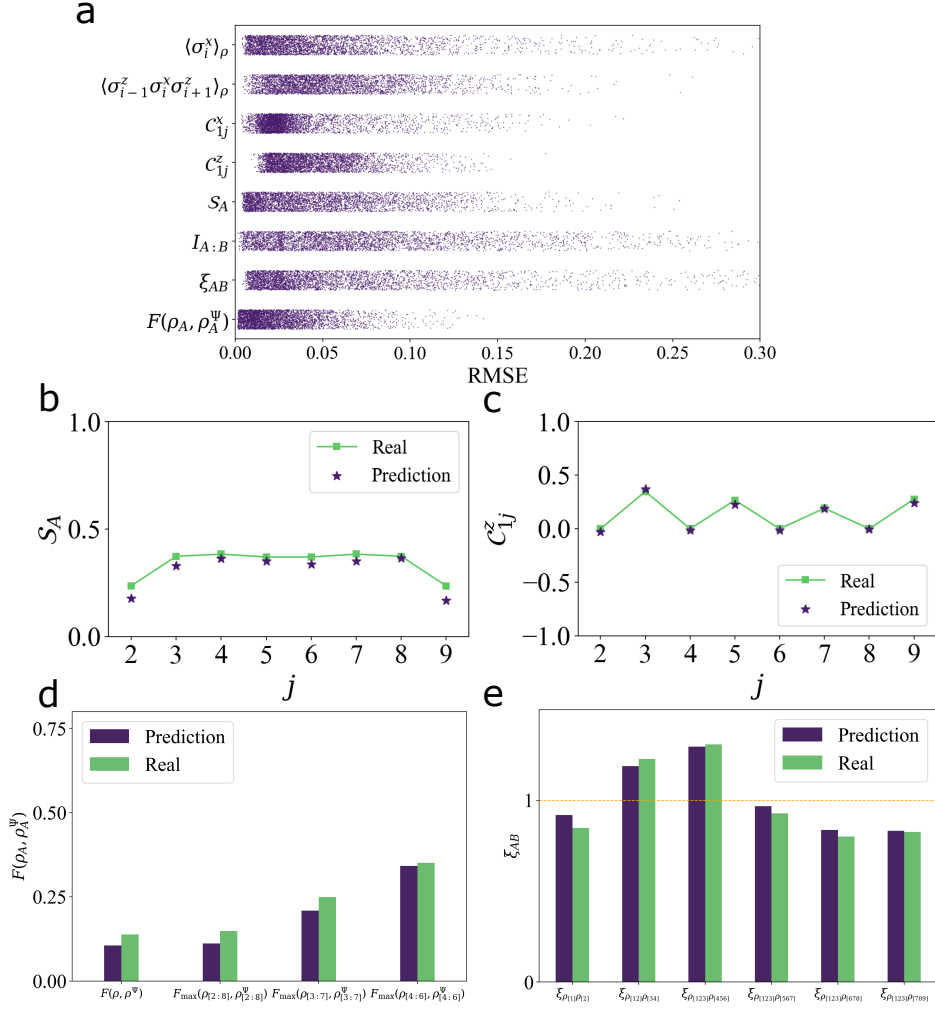


Figure 2. Predicting properties of ground states of cluster-Ising model. Figure **a** illustrates the RMSEs for predicting quantum properties including Pauli expectation values $\langle \sigma_i^x \rangle$ and $\langle \sigma_{i-1}^z \sigma_i^x \sigma_{i+1}^z \rangle$, two-point correlation functions C_{1j}^x and C_{1j}^z , entanglement entropy S_A , mutual information $I_{A:B}$, ratio of partial transpose moments ξ_{AB} and quantum fidelity $F(\rho_A, \rho_A^\Psi)$. RMSE for $\langle \sigma_i^x \rangle$ and $\langle \sigma_{i-1}^z \sigma_i^x \sigma_{i+1}^z \rangle$, C_{1j}^x , C_{1j}^z and S_A are averaged over all i or j . ξ_{AB} is average over the following cases of subsystems: $A = [1], B = [2]$; $A = [12], B = [34]$; $A = [123], B = [456]$; $A = [123], B = [567]$; $A = [123], B = [678]$; $A = [123], B = [789]$. RMSE for $I_{A:B}$ is averaged over the following cases: $A = [123], B = [456]$; $A = [234], B = [678]$; $A = [345], B = [678]$. RMSE for $F(\rho_A, \rho_A^\Psi)$ is average over cases $A = [1 : 9]$, $A = [2 : 8]$, $A = [3 : 7]$ and $A = [456]$. Figures b, c, d and e show the predictions of S_A , C_{1j}^z , $F(\rho_A, \rho_A^\Psi)$, and ξ_{AB} for a ground state corresponding to the Hamiltonian parameters marked by a red star in Fig. **3b**.

Quantitatively, the values of the string order parameter can be extracted from the state representation using another neural network \mathcal{N} . To train this network, we randomly pick 100 reference states $\{\sigma_i\}$ out of the 300 fiducial states and minimize the error $\sum_{i=1}^{100} |\mathcal{N}(\mathbf{r}_{\sigma_i}) - \langle \tilde{S} \rangle_{\sigma_i}|$. Then, we use the trained neural network \mathcal{N} to produce the prediction $\mathcal{N}(\mathbf{r}_\rho)$ of $\langle \tilde{S} \rangle_\rho$ for every other state ρ . The prediction for each ground state is shown in the phase diagram (Fig. **3b**), where the 100 reference states are marked by white circles. The predictions are close to the true values of string order parameters in Fig. **3c**. It is important to stress that, while the network \mathcal{N} was trained on values of the string order parameter, the representation network \mathcal{E} was not provided any information about this parameter. Note also that the values of the

Hamiltonian parameters (h_1, h_2) are just provided in the figure for the purpose of visualization: in fact, no information about the Hamiltonian parameters was provided to the network during training or test.

One-dimensional bond-alternating XXZ model. We now show that our neural network model can be used to learn intermediate scale quantum systems. In the following example, we will also show that our model can be used to predict many-body topological properties from few-body measurements. We consider the ground state of a bond-alternating XXZ model [32] on a system of

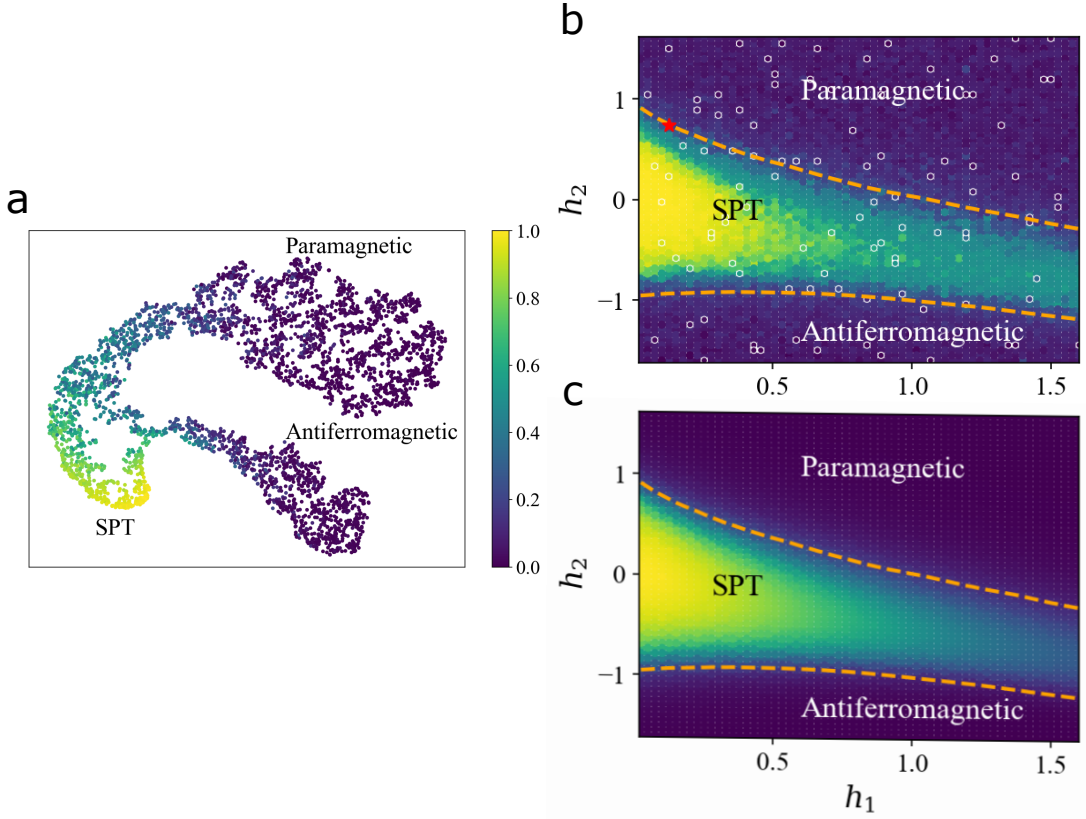


Figure 3. Predicting the phases of cluster-Ising ground states. Subfigure **a** illustrates the 2D projection of the state representations obtained with the t-SNE algorithm. Here, the color of each data point indicates the true value of the string order parameter of the corresponding ground state. Subfigure **b** shows the predictions of string order parameters for 3996 ground states corresponding to the points of a 64×64 grid in parameter space, indicated by the horizontal and vertical axes h_1 and h_2 . The ground states corresponding to 100 randomly chosen points in the grid are used as reference, and the corresponding true values of the string order parameters are indicated by white circles. Subfigure **c** shows the true values of string order parameters of all the ground states. In both **b** and **c**, we show the calculated phase boundaries between SPT phase and the other two phases using dashed curves.

$N = 50$ qubits

$$H = J \sum_{i=1}^{N/2} (\sigma_{2i-1}^x \sigma_{2i}^x + \sigma_{2i-1}^y \sigma_{2i}^y + \delta \sigma_{2i-1}^z \sigma_{2i}^z) + J' \sum_{i=1}^{N/2-1} (\sigma_{2i}^x \sigma_{2i+1}^x + \sigma_{2i}^y \sigma_{2i+1}^y + \delta \sigma_{2i}^z \sigma_{2i+1}^z), \quad (3)$$

where the nearest-neighbour spin coupling strengths are J and J' alternatively. We consider a set of ground states corresponding to a 21×21 square grid in the parameter region $(J/J', \delta) \in (0, 3) \times (0, 4)$. Depending on the ratio of J/J' and the strength of δ , the corresponding ground state falls into one of three possible phases: trivial SPT phase, topological SPT phase, and symmetry broken phase. Unlike the SPT phases of cluster-Ising model, the SPT phases of bond-alternating XXZ model cannot be detected by any string order parameter. Both SPT phases are protected by bond-center inversion symmetry, and detecting them requires a many-body topological invariant, called the partial reflection topological

invariant [32] and denoted by

$$\mathcal{Z}_R := \frac{\text{tr}(\rho_I \mathcal{R}_I)}{\sqrt{[\text{tr}(\rho_{I_1}^2) + \text{tr}(\rho_{I_2}^2)]/2}}. \quad (4)$$

Here, \mathcal{R}_I is the swap operation on subsystem $I := I_1 \cup I_2$ with respect to the center of the spin chain, and $I_1 = [N/2 - 5, N/2 - 4, \dots, N/2]$ and $I_2 = [N/2 + 1, N/2 + 2, \dots, N/2 + 6]$ are two subsystems with six qubits.

We now explore the characterization of the bond-alternating XXZ ground states with our multi-task learning model. For the set of possible measurements \mathcal{M} , we take all possible three-nearest-neighbour Pauli projective measurements, as we did earlier in the cluster-Ising model. For the prediction tasks, we consider two types of quantum properties: (B1) nearest-neighbour spin correlations $\langle \sigma_i^\beta \sigma_{i+1}^\beta \rangle$ ($1 \leq i \leq N - 1$) and next-nearest-neighbour spin correlations $\langle \sigma_i^\beta \sigma_{i+2}^\beta \rangle$ ($1 \leq i \leq N - 2$), where $\beta = x, z$; (B2) order-two Rényi mutual information $I_{A:B}$, where A and B are both 4-qubit subsystems

with the same distance to the center of the spin chain.

We train our neural network with respect to the fiducial ground states corresponding to 80 pairs of $(J/J', \delta)$, randomly sampled from the 441-points grid. For each fiducial state, we provide the neural network with the probability distributions corresponding to $s = 200$ measurements randomly chosen from the 1350 measurements in \mathcal{M} , along with the values of either properties (B1) or properties (B2). After the training is concluded, we use our trained model to predict both properties (B1) and (B2) for all the ground states in the grid. The root mean square error (RMSE) in predicting each property for all the test states are illustrated in Fig. 4a. In most cases, they are below 0.15, indicating a generally good learning performance. Further numerical results are shown in the Supplemental Material.

We show that, even in the larger-scale example considered in this section, the state representations obtained through multi-task training contain information about the quantum phases of matter. In Fig. 4b we show the 2D-projection of the state representations. The data points corresponding to ground states in the trivial SPT phase and in the symmetry broken phase appear to be clearly separated into two clusters, connected by data points corresponding to ground states across the phase boundary. A few points, corresponding to ground states near phase boundaries of the topological SPT phase, are incorrectly clustered by the t-SNE algorithm. The origin of the problem is that the correlation length of ground states near phase boundary becomes longer, and therefore the measurement statistics on nearest-neighbour-three qubit subsystems cannot capture sufficient information for predicting the correct phase of matter.

The emergence of clusters related to different phases of matter suggests that the state representation produced by our network also contains quantitative information about the partial reflection topological invariant \mathcal{Z}_R . To extract this information, we use an additional neural network, which maps the state representation into a prediction of \mathcal{Z}_R . We train this additional network by randomly selecting 60 reference states (marked by grey squares in Fig. 5a and c) out of the set of 441 fiducial states, and by minimizing the prediction error on the reference states. The predictions together with 60 exact values of the reference states are shown in Fig. 5a. The true values of topological invariant are presented in Fig. 5b and the absolute values of the differences between the predictions and ground truths are shown in Fig. 5c. The predictions are close to the ground truths, except for the ground states near the phase boundaries, especially the boundary of topological SPT phase.

In fact, even the boundaries between different phases of matter can be accurately extracted from the state representations, if the value of the Hamiltonian parameters associated with each ground state is available. In order to find all phase boundaries, we adopt a strategy known as learning by confusion [16]. We first propose a hypothesis phase diagram and label the values of \mathcal{Z}_R for 60 refer-

ence states accordingly. Then, we train a neural network using the hypothesized labels to predict the values of \mathcal{Z}_R for all other test states. In the Supplemental Material we show several different hypothesis phase diagrams and the associated prediction results, and we find that only when the hypothesis phase diagram matches the ground truth, the resulting predictions achieve the highest prediction accuracy with respect to the hypothesis. In this way, the unknown phase boundaries can be discovered in a trial-and-error fashion, by finding the hypothesis that maximizes the prediction accuracy.

III. DISCUSSION

We now discuss the differences between our work and related approaches to quantum state characterization. The first difference is that our work addresses the simultaneous prediction of multiple quantum properties using multi-task neural networks. A benefit of this multi-task approach is that the state representations built by our network can capture features of the quantum states that are generally difficult to detect. For example, state representations generated from local measurement data can be used to predict global properties, such as string order parameters and many-body topological invariants. Moreover, they enable unsupervised classification of SPT phases and symmetry broken phases. The ability to capture global features from a small subset of local measurements is a significant difference with most previous works, including shadow tomography approaches [33–35] and machine learning algorithms [1–4, 14].

Another difference is that our model can be used with data from quantum states that were not encountered during training, as long as the test states share similar physical structures with the training states, such as being ground states of Hamiltonians in the same phase of matter. This ability to generalize from a set of quantum states to another does not arise in most approaches based on classical shadow tomography [34, 36, 37] or randomized measurements [30–32, 38, 39]. Our neural network is also quite flexible in terms of data type. While in this paper we focused on multiqubit systems, the network can also be used to learn continuous-variable quantum states, some examples of which are provided in the Supplemental Material.

Overall, our work paves the way to exploring the interactions between different quantum properties in the development of data-driven representations of quantum states. This exploration also provides insights into the amount of local information required to learn global properties, and can shed light on how neural networks can discover physical concepts without any prior knowledge of human-made physical theories.

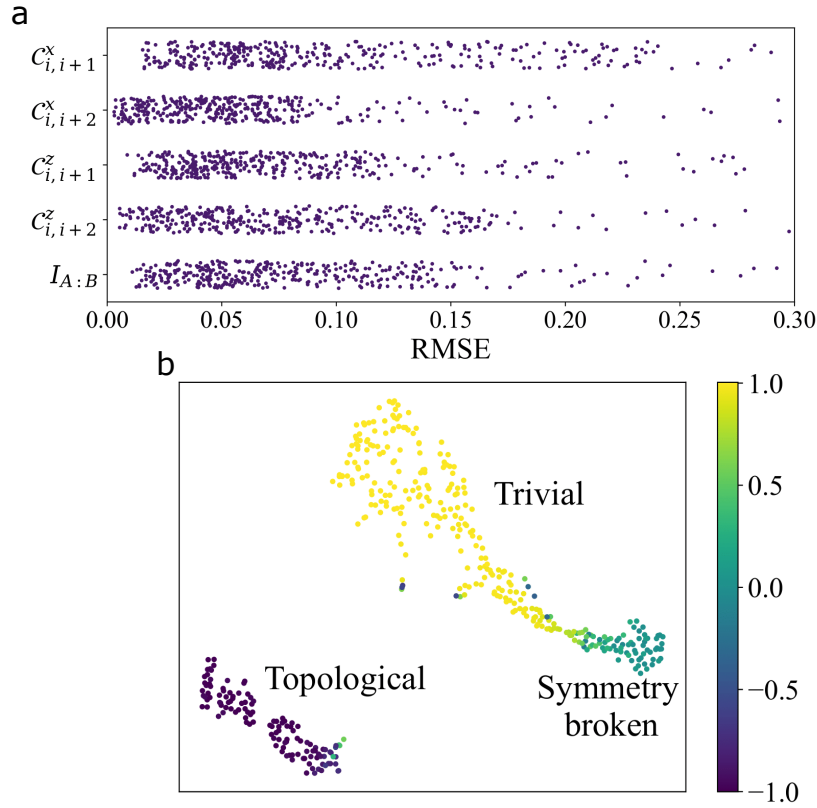


Figure 4. Learning ground state properties in the 50 qubit bond-alternating XXZ model. Subfigure a shows the RMSEs of the predictions of quantum properties $C_{i,i+1}^x$ and $C_{i,i+1}^z$ averaged over all $1 \leq i \leq N-1$, $C_{i,i+2}^x$ and $C_{i,i+2}^z$ averaged over all $1 \leq i \leq N-2$ and $I_{A:B}$ averaged over the different cases of subsystems: $A = [22 : 25]$, $B = [26 : 29]$; $A = [18 : 21]$, $B = [30 : 33]$; $A = [14 : 17]$, $B = [34 : 37]$; and $A = [10 : 13]$, $B = [38 : 41]$. Subfigure b illustrates the 2D projections of the state representations obtained with the t-SNE algorithm. At each data point, we also show the true value of the many-body topological invariant \mathcal{Z}_R of the corresponding ground state.

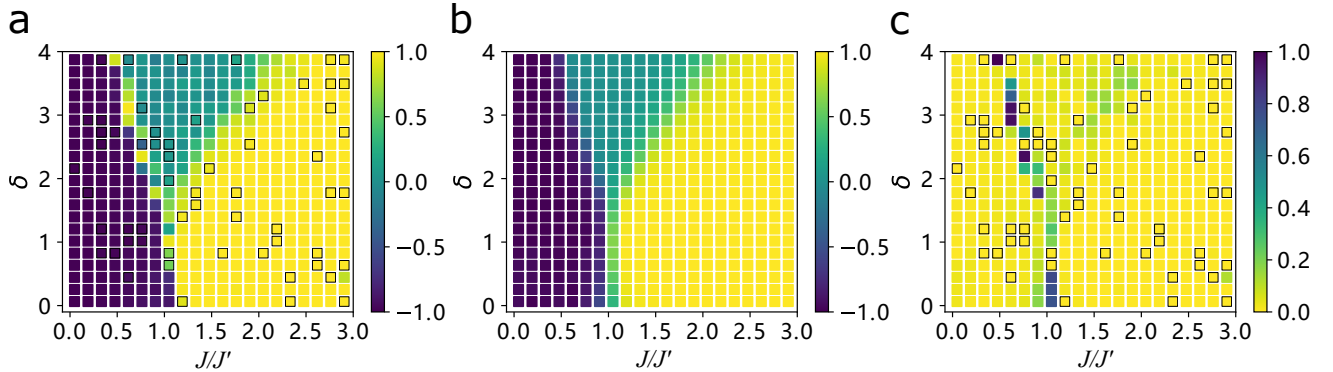


Figure 5. Predictions of the partial reflection topological invariant \mathcal{Z}_R with respect to all pairs of parameters $(J/J', \delta)$ and the corresponding calculated ground truths. Subfigure a shows the predictions produced by the neural network and the true values of 60 reference states marked by grey squares, Subfigure b shows the ground truths and Subfigure c shows the absolute values of the differences between predictions and true values.

IV. METHODS

Data generation. Here we illustrate the procedures for generating training and test datasets. For the one-dimensional cluster-Ising model, we obtain measurement

statistics and values for various properties in both the training and test datasets through direct calculations, leveraging the ground states solved by exact algorithms. In the case of the one-dimensional bond-alternating XXZ model, we first obtain approximate ground states rep-

resented by matrix product states [40, 41] using the density-matrix renormalization group (DMRG) [42] algorithm. Subsequently, we compute the measurement statistics and properties by contracting the tensor networks. The details are provided in SM.

Representation Network. The representation network operates on pairs of measurement outcome distributions and the parameterization of their corresponding measurements, denoted as $(\mathbf{d}_i, \mathbf{m}_i)_{i=1}^m$ associated with a state ρ . This network primarily consists of three multilayer perceptrons (MLPs) [43]. The first MLP comprises a four-layer architecture that transforms the measurement outcome distribution into \mathbf{h}_i^d , whereas the second three-layer MLP maps the corresponding \mathbf{m}_i to \mathbf{h}_i^m :

$$\begin{aligned}\mathbf{h}_i^d &= \text{MLP}_1(\mathbf{d}_i), \\ \mathbf{h}_i^m &= \text{MLP}_2(\mathbf{m}_i).\end{aligned}$$

Next, we merge \mathbf{h}_i^d and \mathbf{h}_i^m , feeding them into another two-layer MLP to obtain a partial representation denoted as \mathbf{r}_i for the state:

$$\mathbf{r}_\rho^{(i)} = \text{MLP}_3([\mathbf{h}_i^d, \mathbf{h}_i^m]). \quad (5)$$

Following this, we aggregate all the \mathbf{r}_i representations through an average pooling layer to produce the complete state representation, denoted as \mathbf{r}_ρ :

$$\mathbf{r}_\rho = \frac{1}{s} \sum_{i=1}^s \mathbf{r}_i. \quad (6)$$

Alternatively, we can leverage a recurrent neural network equipped with gated recurrent units (GRUs) [44] to derive the comprehensive state representation from the set $\{\mathbf{r}_i\}_{i=1}^m$:

$$\begin{aligned}\mathbf{z}_i &= \text{sigmoid}(W_z \mathbf{r}_\rho^{(i)} + U_z \mathbf{r}_\rho^{(i-1)} + \mathbf{b}_z), \\ \hat{\mathbf{h}}_i &= \tanh(W_h \mathbf{r}_\rho^{(i)} + U_h (\mathbf{z}_i \odot \mathbf{h}_{i-1}) + \mathbf{b}_h), \\ \mathbf{h}_i &= (1 - \mathbf{z}_i) \odot \mathbf{h}_{i-1} + \mathbf{z}_i \odot \hat{\mathbf{h}}_i, \\ \mathbf{r}_\rho &= \mathbf{h}_m,\end{aligned}$$

where W, U, \mathbf{b} are trainable matrices and vectors. The architecture of the recurrent neural network offers a more flexible approach to generate the complete state representation; however, in our experiments, we did not observe

significant advantages compared to the average pooling layer.

Prediction Network. For each type of property associated with the state, we employ a dedicated prediction network responsible for making predictions. Each prediction network is composed of two MLPs. The first MLP takes the query task index q as input and transforms it into a feature vector \mathbf{h}^q . The second MLP operates on the combined feature vectors $[\mathbf{h}^q, \mathbf{r}_\rho]$, where \mathbf{r}_ρ represents the state representation, to produce the prediction $f_q(\rho)$ for the property under consideration:

$$\begin{aligned}\mathbf{h}^q &= \text{MLP}_4(q), \\ f_q(\rho) &= \text{MLP}_5([\mathbf{h}^q, \mathbf{r}_\rho]).\end{aligned}$$

Network training. We employ the stochastic gradient descent [45] optimization algorithm and the Adam optimizer [46] to train our neural network. In our training procedure, for each state within the training dataset, we jointly train both the representation network and the prediction networks associated with one or two types of properties available for that specific state. This training is achieved by minimizing the difference between the predicted values generated by the network and the ground-truth values, thus refining the model's ability to capture and reproduce the desired property characteristics. The detailed pseudocode for the training process can be found in SM.

Hardware. We employ the PyTorch framework [47] to construct the multi-task neural networks in all our experiments and train them with two NVIDIA GeForce GTX 1080 Ti GPUs.

Acknowledgements. We thank Ge Bai, Dong-Sheng Wang, Shuo Yang and Yuchen Guo for the helpful discussions on many-body quantum systems. This work was supported by funding from the Hong Kong Research Grant Council through grants no. 17300918 and no. 17307520, through the Senior Research Fellowship Scheme SRFS2021-7S02, and the John Templeton Foundation through grant 62312, The Quantum Information Structure of Spacetime (qiss.fr). YXW acknowledges funding from the National Natural Science Foundation of China through grants no. 61872318. Research at the Perimeter Institute is supported by the Government of Canada through the Department of Innovation, Science and Economic Development Canada and by the Province of Ontario through the Ministry of Research, Innovation and Science. The opinions expressed in this publication are those of the authors and do not necessarily reflect the views of the John Templeton Foundation.

[1] Giacomo Torlai, Guglielmo Mazzola, Juan Carrasquilla, Matthias Troyer, Roger Melko, and Giuseppe Carleo,

“Neural-network quantum state tomography,” *Nat. Phys.* **14**, 447–450 (2018).

- [2] Juan Carrasquilla, Giacomo Torlai, Roger G Melko, and Leandro Aolita, “Reconstructing quantum states with generative models,” *Nat. Mach. Intell.* **1**, 155–161 (2019).
- [3] Yan Zhu, Ya-Dong Wu, Ge Bai, Dong-Sheng Wang, Yuexuan Wang, and Giulio Chiribella, “Flexible learning of quantum states with generative query neural networks,” *Nat. Commun.* **13**, 6222 (2022).
- [4] Tobias Schmale, Moritz Reh, and Martin Gärttner, “Efficient quantum state tomography with convolutional neural networks,” *NPJ Quantum Inf.* **8**, 115 (2022).
- [5] Giuseppe Carleo and Matthias Troyer, “Solving the quantum many-body problem with artificial neural networks,” *Science* **355**, 602–606 (2017).
- [6] Xiaoqian Zhang, Maolin Luo, Zhaodi Wen, Qin Feng, Shengshi Pang, Weiqi Luo, and Xiaoqi Zhou, “Direct fidelity estimation of quantum states using machine learning,” *Phys. Rev. Lett.* **127**, 130503 (2021).
- [7] Ya-Dong Wu, Yan Zhu, Ge Bai, Yuexuan Wang, and Giulio Chiribella, “Quantum similarity testing with convolutional neural networks,” *Phys. Rev. Lett.* **130**, 210601 (2023).
- [8] Jun Gao, Lu-Feng Qiao, Zhi-Qiang Jiao, Yue-Chi Ma, Cheng-Qiu Hu, Ruo-Jing Ren, Ai-Lin Yang, Hao Tang, Man-Hong Yung, and Xian-Min Jin, “Experimental machine learning of quantum states,” *Phys. Rev. Lett.* **120**, 240501 (2018).
- [9] Johnnie Gray, Leonardo Bianchi, Abolfazl Bayat, and Sougato Bose, “Machine-learning-assisted many-body entanglement measurement,” *Phys. Rev. Lett.* **121**, 150503 (2018).
- [10] Dominik Koutný, Laia Ginés, Magdalena Moczala-Dusanowska, Sven Höfling, Christian Schneider, Ana Predojević, and Miroslav Ježek, “Deep learning of quantum entanglement from incomplete measurements,” *Sci. Adv.* **9**, eadd7131 (2023).
- [11] Giacomo Torlai, Brian Timar, Evert P. L. van Nieuwenburg, Harry Levine, Ahmed Omran, Alexander Keesling, Hannes Bernien, Markus Greiner, Vladan Vuletić, Mikhail D. Lukin, Roger G. Melko, and Manuel Endres, “Integrating neural networks with a quantum simulator for state reconstruction,” *Phys. Rev. Lett.* **123**, 230504 (2019).
- [12] Yulei Huang, Liangyu Che, Chao Wei, Feng Xu, Xinfang Nie, Jun Li, Dawei Lu, and Tao Xin, “Measuring quantum entanglement from local information by machine learning,” arXiv preprint arXiv:2209.08501 (2022).
- [13] Murali K Kurmapu, VV Tiunova, ES Tiunov, Martin Ringbauer, Christine Maier, Rainer Blatt, Thomas Monz, Aleksey K Fedorov, and AI Lvovsky, “Reconstructing complex states of a 20-qubit quantum simulator,” arXiv preprint arXiv:2208.04862 (2022).
- [14] Alistair W. R. Smith, Johnnie Gray, and M. S. Kim, “Efficient quantum state sample tomography with basis-dependent neural networks,” *PRX Quantum* **2**, 020348 (2021).
- [15] Juan Carrasquilla and Roger G Melko, “Machine learning phases of matter,” *Nat. Phys.* **13**, 431–434 (2017).
- [16] Evert PL Van Nieuwenburg, Ye-Hua Liu, and Sebastian D Huber, “Learning phase transitions by confusion,” *Nat. Phys.* **13**, 435–439 (2017).
- [17] Benno S Rem, Niklas Käming, Matthias Tarnowski, Luca Asteria, Nick Fläschner, Christoph Becker, Klaus Sengstock, and Christof Weitenberg, “Identifying quantum phase transitions using artificial neural networks on experimental data,” *Nat. Phys.* **15**, 917–920 (2019).
- [18] Korbinian Kottmann, Patrick Huembeli, Maciej Lewenstein, and Antonio Acín, “Unsupervised phase discovery with deep anomaly detection,” *Phys. Rev. Lett.* **125**, 170603 (2020).
- [19] Yu Zhang and Qiang Yang, “A survey on multi-task learning,” *IEEE Trans. Knowl. Data Eng.* **34**, 5586–5609 (2021).
- [20] Frank Pollmann and Ari M. Turner, “Detection of symmetry-protected topological phases in one dimension,” *Phys. Rev. B* **86**, 125441 (2012).
- [21] Zheng-Cheng Gu and Xiao-Gang Wen, “Tensor-entanglement-filtering renormalization approach and symmetry-protected topological order,” *Phys. Rev. B* **80**, 155131 (2009).
- [22] Frank Pollmann, Erez Berg, Ari M. Turner, and Masaki Oshikawa, “Symmetry protection of topological phases in one-dimensional quantum spin systems,” *Phys. Rev. B* **85**, 075125 (2012).
- [23] Marcus Cramer, Martin B Plenio, Steven T Flammia, Rolando Somma, David Gross, Stephen D Bartlett, Olivier Landon-Cardinal, David Poulin, and Yi-Kai Liu, “Efficient quantum state tomography,” *Nat. Commun.* **1**, 149 (2010).
- [24] Jordan Cotler and Frank Wilczek, “Quantum overlapping tomography,” *Phys. Rev. Lett.* **124**, 100401 (2020).
- [25] Hsin-Yuan Huang, Richard Kueng, Giacomo Torlai, Victor V Albert, and John Preskill, “Provably efficient machine learning for quantum many-body problems,” *Science* **377**, eabk3333 (2022).
- [26] Pietro Smacchia, Luigi Amico, Paolo Facchi, Rosario Fazio, Giuseppe Florio, Saverio Pascasio, and Vlatko Vedral, “Statistical mechanics of the cluster ising model,” *Phys. Rev. A* **84**, 022304 (2011).
- [27] Hans J. Briegel and Robert Raussendorf, “Persistent entanglement in arrays of interacting particles,” *Phys. Rev. Lett.* **86**, 910–913 (2001).
- [28] Iris Cong, Soonwon Choi, and Mikhail D Lukin, “Quantum convolutional neural networks,” *Nat. Phys.* **15**, 1273–1278 (2019).
- [29] Johannes Herrmann, Sergi Masot Llima, Ants Remm, Petr Zapletal, Nathan A McMahon, Colin Scarato, François Swiadek, Christian Kraglund Andersen, Christoph Hellings, Sebastian Krinner, *et al.*, “Realizing quantum convolutional neural networks on a superconducting quantum processor to recognize quantum phases,” *Nat. Commun.* **13**, 4144 (2022).
- [30] Andreas Elben, Richard Kueng, Hsin-Yuan (Robert) Huang, Rick van Bijnen, Christian Kokail, Marcello Dalmonte, Pasquale Calabrese, Barbara Kraus, John Preskill, Peter Zoller, and Benoît Vermersch, “Mixed-state entanglement from local randomized measurements,” *Phys. Rev. Lett.* **125**, 200501 (2020).
- [31] Andreas Elben, Steven T Flammia, Hsin-Yuan Huang, Richard Kueng, John Preskill, Benoît Vermersch, and Peter Zoller, “The randomized measurement toolbox,” *Nat. Rev. Phys.* **5**, 9–24 (2023).
- [32] Andreas Elben, Jinlong Yu, Guanyu Zhu, Mohammad Hafezi, Frank Pollmann, Peter Zoller, and Benoît Vermersch, “Many-body topological invariants from randomized measurements in synthetic quantum matter,” *Sci. Adv.* **6**, eaaz3666 (2020).
- [33] Scott Aaronson, “Shadow tomography of quantum states,” in *Proceedings of the 50th annual ACM SIGACT*

- symposium on theory of computing* (2018) pp. 325–338.
- [34] Hsin-Yuan Huang, Richard Kueng, and John Preskill, “Predicting many properties of a quantum system from very few measurements,” *Nat. Phys.* **16**, 1050–1057 (2020).
 - [35] Hsin-Yuan Huang, “Learning quantum states from their classical shadows,” *Nat. Rev. Phys.* **4**, 81–81 (2022).
 - [36] Andrew Zhao, Nicholas C. Rubin, and Akimasa Miyake, “Fermionic partial tomography via classical shadows,” *Phys. Rev. Lett.* **127**, 110504 (2021).
 - [37] Simon Becker, Nilanjana Datta, Ludovico Lami, and Cambyse Rouzé, “Classical shadow tomography for continuous variables quantum systems,” arXiv preprint arXiv:2211.07578 (2022).
 - [38] Andreas Elben, Benoît Vermersch, Rick van Bijnen, Christian Kokail, Tiff Brydges, Christine Maier, Manoj K. Joshi, Rainer Blatt, Christian F. Roos, and Peter Zoller, “Cross-platform verification of intermediate scale quantum devices,” *Phys. Rev. Lett.* **124**, 010504 (2020).
 - [39] Tiff Brydges, Andreas Elben, Petar Jurcevic, Benoît Vermersch, Christine Maier, Ben P Lanyon, Peter Zoller, Rainer Blatt, and Christian F Roos, “Probing rényi entanglement entropy via randomized measurements,” *Science* **364**, 260–263 (2019).
 - [40] Mark Fannes, Bruno Nachtergaele, and Reinhard F Werner, “Finitely correlated states on quantum spin chains,” *Commun. Math. Phys.* **144**, 443–490 (1992).
 - [41] David Perez-García, Frank Verstraete, Michael M Wolf, and J Ignacio Cirac, “Matrix product state representations,” *Quantum Inf. Comput.* **7**, 401–430 (2007).
 - [42] Ulrich Schollwöck, “The density-matrix renormalization group,” *Rev. Mod. Phys.* **77**, 259 (2005).
 - [43] Matt W Gardner and SR Dorling, “Artificial neural networks (the multilayer perceptron)—a review of applications in the atmospheric sciences,” *Atmospheric environment* **32**, 2627–2636 (1998).
 - [44] Junyoung Chung, Caglar Gulcehre, Kyunghyun Cho, and Yoshua Bengio, “Empirical evaluation of gated recurrent neural networks on sequence modeling,” in *NIPS 2014 Workshop on Deep Learning, December 2014* (2014).
 - [45] Léon Bottou, “Stochastic gradient descent tricks,” in *Neural Networks: Tricks of the Trade: Second Edition* (Springer, 2012) pp. 421–436.
 - [46] Diederik P Kingma and Jimmy Ba, “Adam: A method for stochastic optimization,” arXiv preprint arXiv:1412.6980 (2014).
 - [47] Adam Paszke, Sam Gross, Francisco Massa, Adam Lerer, James Bradbury, Gregory Chanan, Trevor Killeen, Zeming Lin, Natalia Gimelshein, Luca Antiga, *et al.*, “Pytorch: An imperative style, high-performance deep learning library,” *Advances in neural information processing systems* **32** (2019).